Acceleration of the Brewer–Dobson Circulation due to Increases in Greenhouse Gases

ROLANDO R. GARCIA AND WILLIAM J. RANDEL

National Center for Atmospheric Research, Boulder, Colorado*

(Manuscript received 11 December 2007, in final form 16 January 2008)

ABSTRACT

The acceleration of the Brewer–Dobson circulation under rising concentrations of greenhouse gases is investigated using the Whole Atmosphere Community Climate Model. The circulation strengthens as a result of increased wave driving in the subtropical lower stratosphere, which in turn occurs because of enhanced propagation and dissipation of waves in this region. Enhanced wave propagation is due to changes in tropospheric and lower-stratospheric zonal-mean winds, which become more westerly. Ultimately, these trends follow from changes in the zonal-mean temperature distribution caused by the greenhouse effect. The circulation in the middle and upper stratosphere also accelerates as a result of filtering of parameterized gravity waves by stronger subtropical westerly winds.

1. Introduction

A robust result of simulations of the atmospheric response to increases in greenhouse gases (GHG) is the acceleration of the stratospheric mean meridional, or Brewer–Dobson (BD), circulation (e.g., Butchart and Scaife 2001; Rind et al. 2001; Sigmond et al. 2004; Butchart et al. 2006; Eichelberger and Hartmann 2005; Olsen et al. 2007). A stronger BD circulation leads to changes in the transport of stratospheric tracers and in the stratospheric "age of air" (AOA) (Hall and Plumb 1994), which becomes progressively younger as GHG concentrations increase (Austin and Li 2006; Garcia et al. 2007).

The acceleration of the BD circulation has been attributed to increases in wave driving due to stronger wave excitation as the troposphere warms in response to higher concentrations of GHG (see Butchart et al. 2006, and references therein). There is, however, no general agreement on which waves might be most important or whether the waves act mainly in the subtropics or in mid- and high latitudes. For example, Olsen et al. (2007) suggest that waves are refracted poleward and produce enhanced forcing in the polar stratosphere, whereas Fomichev et al. (2007) emphasize increases of wave driving at subtropical latitudes. Still other studies do not indicate a significant change in wave activity (Sigmond et al. 2004).

Here we use simulations carried out with the Whole Atmosphere Community Climate Model to elucidate the mechanism that produces changes in the BD circulation under increasing GHG loading. It is shown that acceleration of the BD circulation is a robust result of the simulations, and that it may be understood to arise from changes in the zonal-mean zonal wind structure of the tropical and subtropical lower stratosphere, which allow enhanced propagation and dissipation of wave activity in this region. Since the zonal-mean wind is in geostrophic balance with the zonal-mean temperature, changes in the BD circulation are ultimately attributable to the temperature trends brought about by increasing GHG.

2. Numerical model and simulations

The simulations discussed below use version 3 of the Whole Atmosphere Community Climate Model (WACCM3), developed at the National Center for Atmospheric Research (NCAR), which has been described in detail by Garcia et al. (2007). WACCM3 is a fully coupled chemistry–climate model (CCM) that spans the altitude range 0–140 km, with vertical reso-

* The National Center for Atmospheric Research is sponsored by the National Science Foundation.

Corresponding author address: Rolando R. Garcia, National Center for Atmospheric Research, P.O. Box 3000, Boulder, CO 80307-3000.
E-mail: rgarcia@ucar.edu

DOI: 10.1175/2008JAS2712.1

lution of ~1.25 km in the troposphere and lower stratosphere, decreasing to 1.75 km in the upper stratosphere and about 3.5 km in the upper mesosphere and thermosphere. All of the runs presented here were made at horizontal resolution of 4° latitude by 5° longitude. The simulations were part of the CCM validation activity of the Stratospheric Processes and their Role in Climate (SPARC) project and have been described in detail by Eyring et al. (2006, 2007) and (specifically for WACCM3) Garcia et al. (2007).

Three simulations, each consisting of three ensemble members, were carried out. The first, or reference simulation 1 (REF1), is a "retrospective" simulation of the twentieth century (1950–2003), with sea surface temperatures (SST) and loadings of GHG and halogen species specified from observations. The second simulation, reference simulation 2 (REF2), is a prognostic run spanning the years 1980–2050 and is designed to study ozone recovery in the twenty-first century. REF2 was carried out with GHG [carbon dioxide (CO_2), methane (CH_4), and nitrous oxide (N_2O)] and halogen abundances recommended by the Intergovernmental Panel for Climate Change (IPCC scenario A1b; Houghton et al. 2001) and the World Meteorological Organization (Table 4B-2 of WMO 2003), respectively. SST were specified from a run made with NCAR's Community Atmosphere Model (CAM3), upon which WACCM3 is based, coupled to a full ocean and with the abundances of GHG also specified according to scenario A1b of IPCC. The last simulation is similar to REF2 except that the concentrations of CO_2, CH_4, and N_2O were held at 1995 values from 1995 to 2050 for the purpose of assessing the impact of GHG-induced climate change on ozone recovery by comparison with REF2. This run, the "no climate change" (NCC) simulation, used SST specified from a coupled CAM3 run in which GHG were also held constant after 1995.

Garcia et al. (2007) showed that the stratospheric AOA in REF1 decreased by about 2% $(10\ \text{yr})^{-1}$ from 1960 to 2003, consistent with the mean AOA decrease found by Butchart et al. (2006) in their intercomparison of the response of the BD circulation to increases in CO_2 in several CCM. Figure 1 shows the ensemble-mean evolution of tropical-mean AOA at 10 hPa in the REF1 simulation, as well as in REF2 and NCC. It is apparent that AOA decreases steadily in the two simulations with increasing GHG, but it undergoes no significant change in NCC, wherein GHG are held constant. The rate of decrease of AOA is similar in REF1 and REF2, notwithstanding the fact that REF1 spanned the period of formation of the stratospheric "ozone hole," whereas REF2 covered the period of ozone recovery in the twenty-first century, suggesting that the behavior of polar ozone is not crucial to the changes in the BD circulation. The total decrease of AOA over the nine decades spanned by these two simulations is approximately 20%. In the remainder of the paper, we focus on the behavior of AOA and other relevant atmospheric fields in simulations REF1 and REF2.

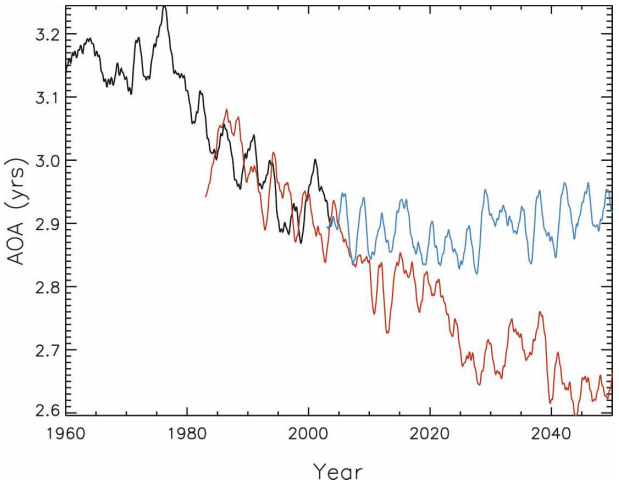

FIG. 1. Evolution of the age of air near 10 hPa averaged over ±22° [months $(10\ \text{yr})^{-1}$] for three-member ensemble simulations of the climate of the twentieth century (REF1; black curve); the climate of the twenty-first century under increasing loading of GHG (REF2; red); and the climate of the twenty-first century with GHG held constant at 1995 values (NCC; blue). See text for details.

3. Analysis

Figure 2 shows the distribution of the ensemble-mean trend in AOA for simulations REF1 and REF2. This and other trends shown in this paper are obtained by regression of deseasonalized monthly- and zonal-mean model output smoothed with a 3-month boxcar average, and the resulting regression coefficients are shown as functions of latitude and altitude. Superimposed upon the AOA trend [months $(10\ \text{yr})^{-1}$] is the ensemble-mean trend in the vector transformed Eulerian mean (TEM) meridional circulation ($\overline{v}^*$, $\overline{w}^*$) (Andrews et al. 1987). Note that the BD circulation is envisaged as the Lagrangian-mean motion of air parcels in the stratosphere and therefore cannot be calculated with an Eulerian numerical model; however, as discussed by Andrews et al., the TEM circulation is a good approximation thereof.

The striking feature of Fig. 2 is the very sharp gradient in AOA trend in the tropical lower stratosphere, which is accompanied by the largest trends in ($\overline{v}^*$, $\overline{w}^*$) in both REF1 and REF2. There are large trends in ($\overline{v}^*$, $\overline{w}^*$) elsewhere, including the tropics in the upper strato-

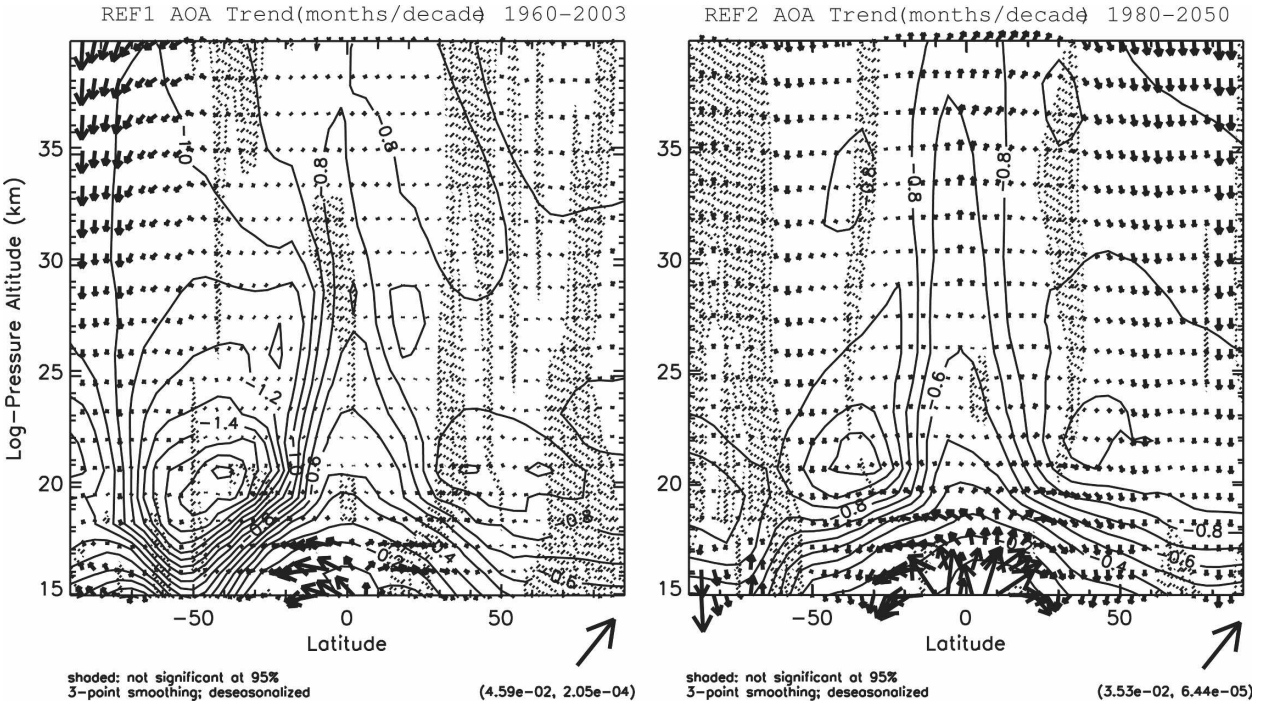

FIG. 2. Ensemble-mean trends of age of air [months $(10\ \mathrm{yr})^{-1}$] for the (left) REF1 and (right) REF2 simulations. The trends in vector TEM meridional circulation [contour interval is 0.1 m s^{-1} $(10\ \mathrm{yr})^{-1}$] are superimposed. All trends are obtained by regression upon time of deseasonalized zonal- and monthly-mean model results smoothed with a 3-month boxcar average. Stippling indicates where trends are not significant at the 2-σ level; the arrow on the lower-right-hand corner indicates the scale of the vector trend. See text for details.

sphere, broad regions of the midlatitudes above 25 km, and the southern polar cap (especially in simulation REF1). The southern polar cap trends are associated with the formation and recovery of the ozone hole in REF1 and REF2, respectively; the midlatitude trends above 25 km are the result of increases in parameterized gravity wave drag, as will be shown below. These exceptions notwithstanding, it is evident that in WACCM3 the acceleration of the BD circulation and the decrease in stratospheric AOA are associated principally with the behavior in the tropical lower stratosphere, between the tropopause and about 20–22-km altitude (~50 hPa); it is shown next that these trends are due to an increase in Eliassen–Palm (EP) flux divergence due to waves resolved in the model.

Figure 3 shows the ensemble-mean trend in vector EP flux **F** for waves that are explicitly resolved in WACCM3 superimposed on the corresponding trend in the wave-induced zonal-mean acceleration, $(\rho a \cos\theta)^{-1}$ $\nabla \cdot \mathbf{F}$, where ρ is the density, θ is the latitude, and a is the radius of the earth. There are two statistically significant regions of enhanced acceleration in the subtropical lower stratosphere, centered at approximately $\pm 25°$ and 16–17 km. These acceleration anomalies drive the trends in $(\bar{v}^*, \bar{w}^*)$ and AOA illustrated in Fig. 2. This may be verified by comparison with that figure, where the largest $\bar{v}^*$ trends coincide with the largest trends in wave-induced acceleration in Fig. 3, as expected from the steady-state TEM momentum equation, $-f\bar{v}^* \simeq (\rho a \cos\theta)^{-1} \nabla \cdot \mathbf{F}$, where f is the Coriolis parameter. Other locations where the trend in wave-induced acceleration is both large and statistically significant include some midlatitude regions above ~25 km. These midlatitude trends are not always consistent with the trend in $\bar{v}^*$ at the same locations. For example, in REF2 the maximum in wave-induced acceleration at 50°–55°N in the middle and upper stratosphere coincides with an increase in $\bar{w}^*$ rather than with a change in $\bar{v}^*$ as would be expected from the steady-state momentum balance; thus, the changes in the mean meridional circulation in this region must be driven mainly by another forcing mechanism, such as the dissipation of (parameterized) gravity waves.

It remains now to attribute quantitatively the changes in $(\bar{v}^*, \bar{w}^*)$ to wave driving in WACCM3. This may be done succinctly by using the "downward control principle" (Haynes et al. 1991) to estimate the vertical component of the TEM circulation averaged over the tropical ascent region in the stratosphere. As shown by Randel et al. (2002), it is straightforward to derive an expression for the area-weighted, meridional average of $\bar{w}^*$ between latitudes $\pm\theta_0$:

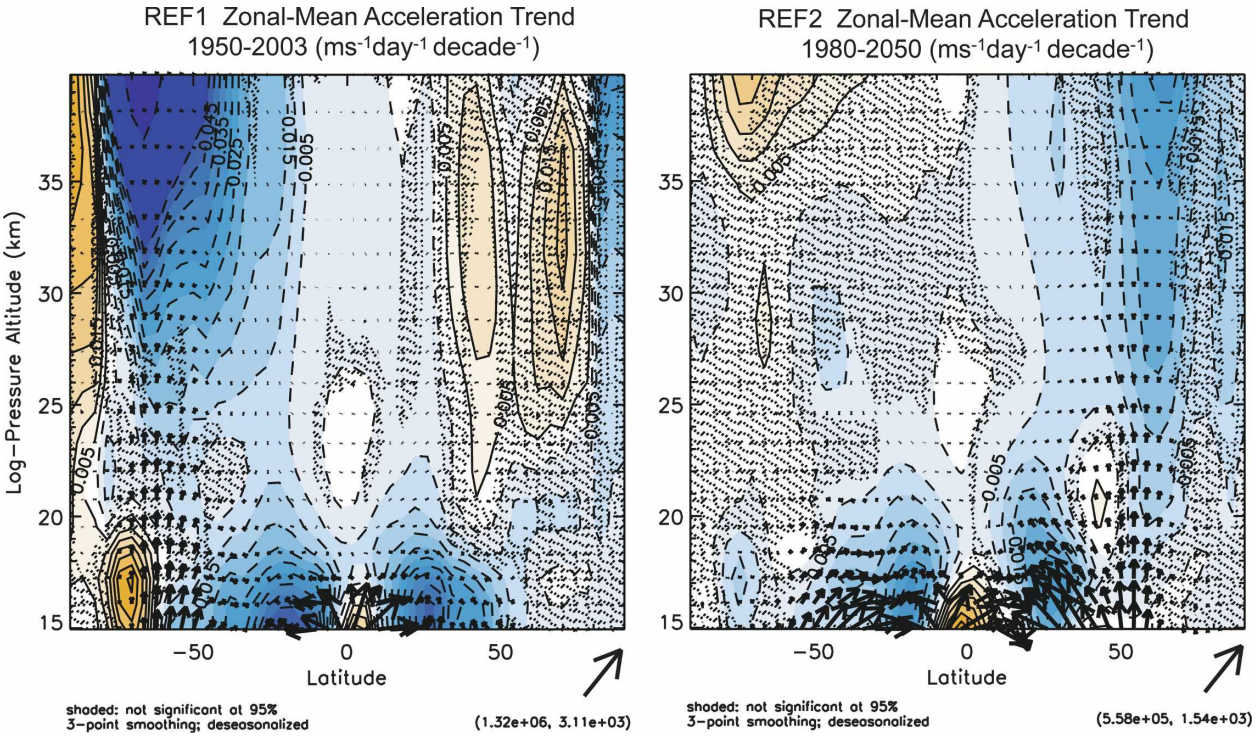

FIG. 3. As in Fig. 2, but for the ensemble-mean trends in zonal-mean acceleration due to resolved waves [contour interval is 0.005 m s^{-1} day^{-1} (10 yr)$^{-1}$], with the trends in vector EP flux [kg s^{-2} (10 yr)$^{-1}$] superimposed. Vector EP flux is plotted as $\cos\theta(a^{-1}\mathbf{F}_y, \mathbf{F}_z)$, where θ is latitude and a is the earth's radius, which makes the pattern appear nondivergent in the (θ, z) plane when the flux divergence vanishes (Edmon et al. 1980).

$$\langle\overline{w}^*\rangle(z) = \frac{\left|\dfrac{1}{\rho(z)}\displaystyle\int_z^\infty \frac{\rho a\cos^2\theta[(\rho a\cos\theta)^{-1}\nabla\cdot\mathbf{F}(\theta,z')] + \mathbf{X}(\theta,z')}{\overline{m}_\theta}\,dz'\right|_{-\theta_0}^{+\theta_0}}{|\sin\theta|_{-\theta_0}^{+\theta_0}}, \tag{1}$$

where z is log-pressure altitude, $\overline{m} = a\cos\theta(\overline{u} + \Omega a\cos\theta)$ is the zonal-mean angular momentum, including the contribution of the earth's rotation Ω, and $\mathbf{X}$ denotes the zonal force due to unresolved waves, which in WACCM3 is calculated from a parameterization of mesoscale gravity waves (Garcia et al. 2007). Here we take $\theta_0 = 22°$, which encompasses approximately the stratospheric upwelling region in WACCM3, and evaluate the integrand of Eq. (1) at constant latitudes rather than along contours of constant $\overline{m}$ as would be strictly correct, because the contours of $\overline{m}$ are approximately vertical for our choice of θ_0.

The black curve in Fig. 4 shows the vertical profile of the ensemble-mean trend in $\langle\overline{w}^*\rangle$ for simulation REF2 calculated taking into account the contribution of the trends in both resolved and parameterized waves; these values are everywhere within ~15% of those obtained by averaging the actual trend of $\overline{w}^*$ across the tropics (shown by the dashed curve in the figure), confirming the applicability of the downward control principle to the present problem. The red curve in Fig. 4 shows the trend in $\langle\overline{w}^*\rangle$ computed without the contribution of parameterized gravity waves. It is clear that the latter is small below ~20–22 km but becomes increasingly important above that altitude and is dominant in the upper stratosphere. This is consistent with the remark made above that the trend in resolved wave-induced acceleration cannot account for the trend in the TEM circulation in the middle and upper stratosphere. Figure 4 shows that it is instead the trend in $\mathbf{X}$ that drives the change in $(\overline{v}^*, \overline{w}^*)$ and AOA in this region. Similar results, for both the magnitude of the trend in tropical upwelling and the relative contribution of parameterized gravity waves, are obtained for simulation REF1 (not shown).

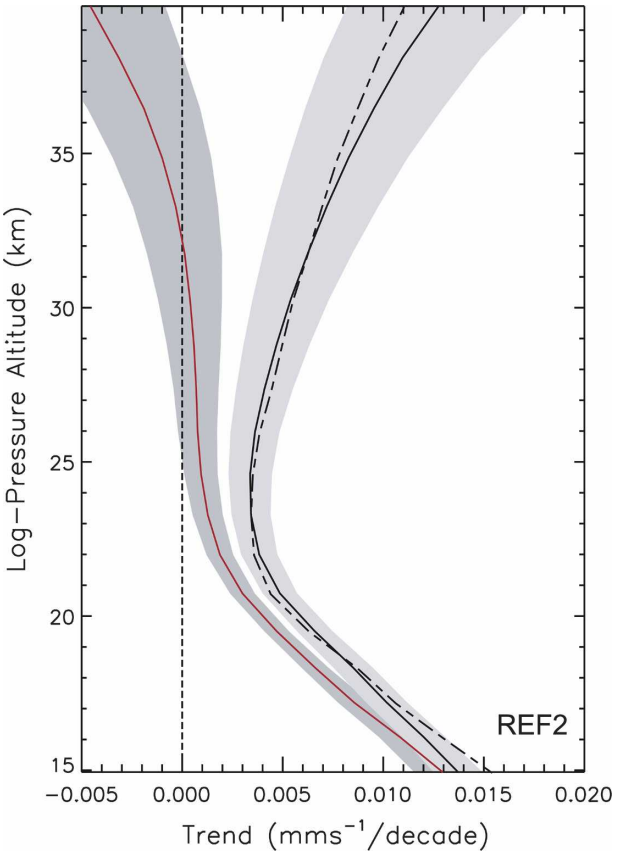

FIG. 4. Ensemble-mean trend of the TEM vertical velocity averaged over ±22° [mm s^{-1} (10 yr)$^{-1}$] for simulation REF2 calculated from the downward control principle. The black curve shows the results including resolved and parameterized waves; the red curve omits parameterized waves. Shadowing indicates the 2-σ confidence limits. For comparison, the dashed curve shows the trend of the actual TEM vertical velocity averaged over ±22°. See text for details.

4. Discussion

Figures 2–4 support the conclusion that in WACCM3 the acceleration of the BD circulation under increasing concentrations of GHG follows from changes in wave driving by explicitly resolved waves in the subtropical lower stratosphere and by (parameterized) mesoscale gravity waves at higher altitudes. A remaining question is what causes these trends in wave driving. We find no clear evidence of an increase in wave excitation, as determined by examining changes in the vertical component of resolved EP flux F_z emerging from the lower troposphere. In the model, $\nabla \cdot \mathbf{F}$ is positive (indicative of wave generation) almost everywhere in the lower troposphere below about 5–6 km, and is negative (consistent with wave dissipation) throughout most of the upper troposphere and the stratosphere; consequently, F_z is positive (upward) irrespective of latitude in the model troposphere, as shown in Fig. 5. In the upper troposphere (8–12 km), above the region of wave generation, the latitude average of the trend in F_z is on the order of 0.1% (10 yr)$^{-1}$, which may be interpreted as evidence of negligible change in the generation of vertically propagating wave activity.

What instead appears to happen in WACCM3 is that a greater fraction of vertically propagating wave activity reaches the stratosphere and, in particular, the subtropical stratosphere between 15 and 20 km, where it dissipates. These regions of enhanced dissipation represent an intensification and upward extension in the lower stratosphere of the time-mean pattern of wave-induced acceleration shown in Fig. 5, and they are associated with changes in the structure of the zonal-mean winds in the upper troposphere and lower stratosphere, as illustrated in Fig. 6, which shows the behavior of the trends in zonal-mean zonal wind and vector EP flux. There is an enhancement of the EP flux reaching the lower stratosphere wherever the trend in zonal wind is large and positive. The divergence of this EP flux, which was shown in Fig. 3, then drives the trend in the BD circulation. The spatial pattern of the EP flux trend differs between the REF1 and REF2 simulations. In the former, the greatest enhancement of EP flux entering the stratosphere occurs in the tropics, while in the latter it occurs at midlatitudes; however, in both cases these enhancements coincide with the largest positive (westerly) trends in the zonal-mean zonal wind.

The increase in parameterized gravity wave drag responsible for the circulation trends in the middle and upper stratosphere (cf. Figs. 2, 4) also arises from changes in the zonal wind distribution in the lower stratosphere, because these affect the dissipation of the orographic component of the gravity wave spectrum. In effect, less of the wave activity associated with this parameterized wave is dissipated in the lower stratosphere, where the zonal-mean winds become stronger, and more is dissipated at higher altitudes.

The role of the subtropical lower stratosphere in the acceleration of the BD circulation has been emphasized in other recent studies. For example, Eichelberger and Hartmann (2005) noted the increase in the subtropical temperature gradient, and argued that it enhanced the generation of wave activity through an increase in the baroclinicity of the troposphere. Olsen et al. (2007) also pointed out that tropospheric warming leads to a greater meridional temperature gradient in the subtropics, accelerating the winds there and leading to refraction of upward-propagating waves toward high lati-

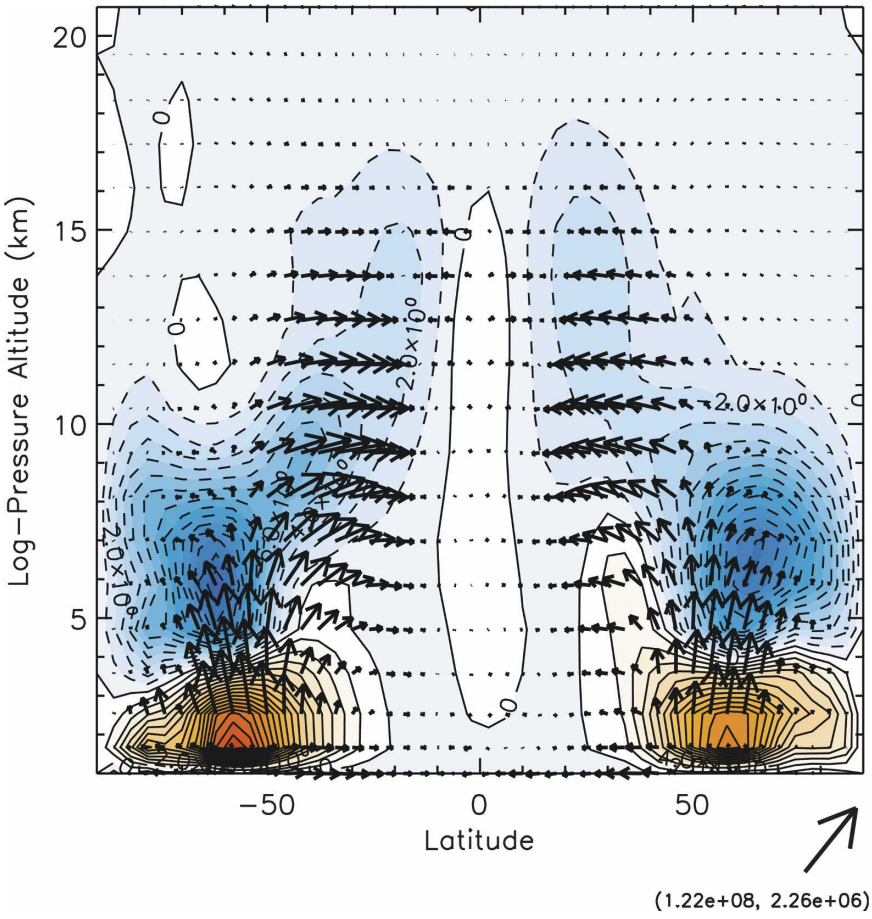

FIG. 5. Ensemble-mean, time-mean pattern of EP flux divergence (contour interval is 1 m s^{-1} day^{-1}) and vector EP flux (kg s^{-2}) for simulation REF2. Vector EP flux is plotted using the convention of Edmon et al. (1980).

tudes. The results presented here support the importance of zonal wind trends but with a different emphasis than the aforementioned studies. In WACCM3 there does not appear to be much change in the generation of wave activity, nor are changes in wave propagation most important at polar latitudes. Instead, the trends in the circulation arise from enhanced propagation of wave activity into the lower stratosphere and its dissipation in the subtropics. In this regard, the conclusions presented here are closest to those of Fomichev et al. (2007), who showed that, in their model, changes in wave driving at lower latitudes (20°–40°) must be responsible for the circulation trends they obtained. The results of the multimodel comparison by Butchart et al. (2006) are also consistent with the present results, insofar as these authors applied a variant of the downward control principle to obtain results analogous to those shown in our Fig. 4.

The zonal wind trends illustrated in Fig. 6 are geostrophically consistent with the corresponding trends in temperature, as can be seen by comparing that figure with Fig. 7, which shows the zonal-mean temperature trends. In particular, the meridional gradient of temperature steepens in the subtropical upper troposphere and lower stratosphere because this is the region of largest temperature contrast between the tropical troposphere (which warms in response to increasing GHG) and the lowermost extratropical stratosphere (which becomes cooler). In addition, in the REF1 simulation the temperature trend in the troposphere has a relatively strong meridional gradient in the deep tropics. Because of the smallness of the Coriolis parameter near the equator, this translates into the large tropical trend in zonal-mean wind seen in Fig. 5. Because the trends in the meridional temperature gradient in the upper troposphere and lower stratosphere (and the corresponding westerly zonal wind trends) are a direct response to GHG increases, one would expect that enhanced propagation of wave activity into the lower stratosphere should be a robust response to GHG

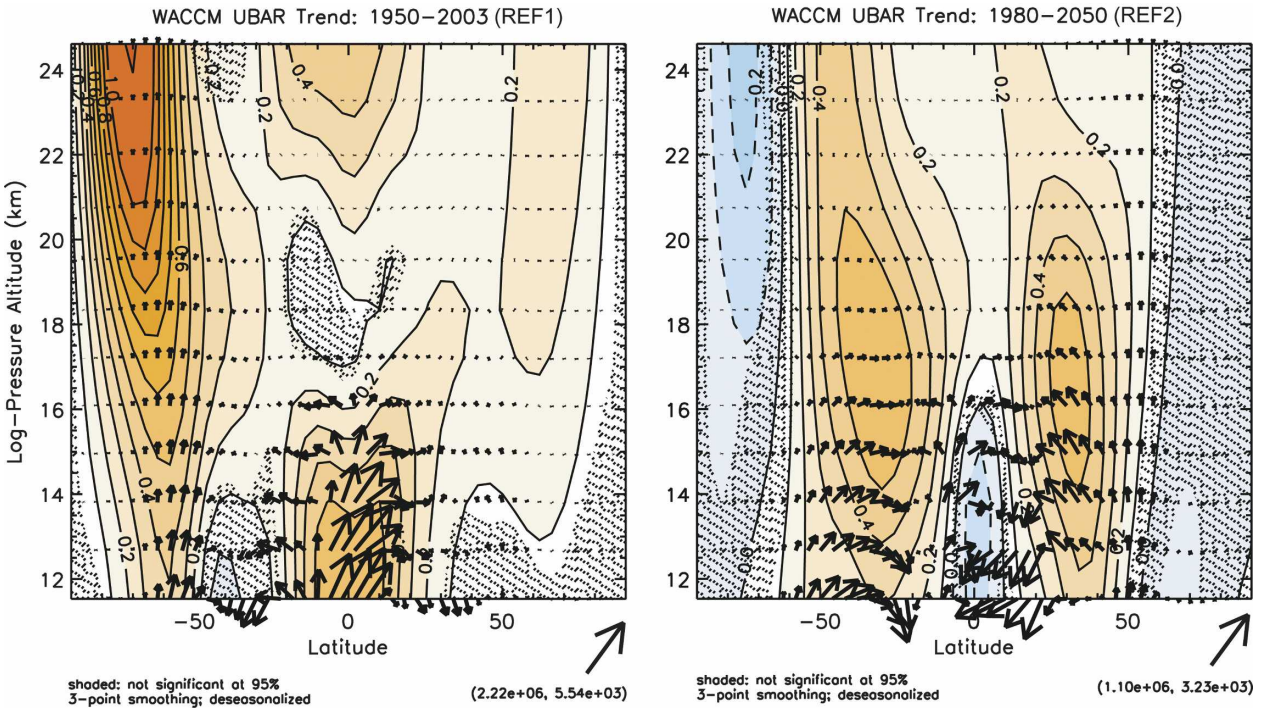

FIG. 6. As in Fig. 2, but for the ensemble-mean trends in zonal-mean zonal wind [contour interval is 0.1 m s^{-1} (10 yr)$^{-1}$] in the upper troposphere and lower stratosphere, with the trends in vector EP flux [kg s^{-2} (10 yr)$^{-1}$] superimposed. Vector EP flux is plotted using the convention of Edmon et al. (1980).

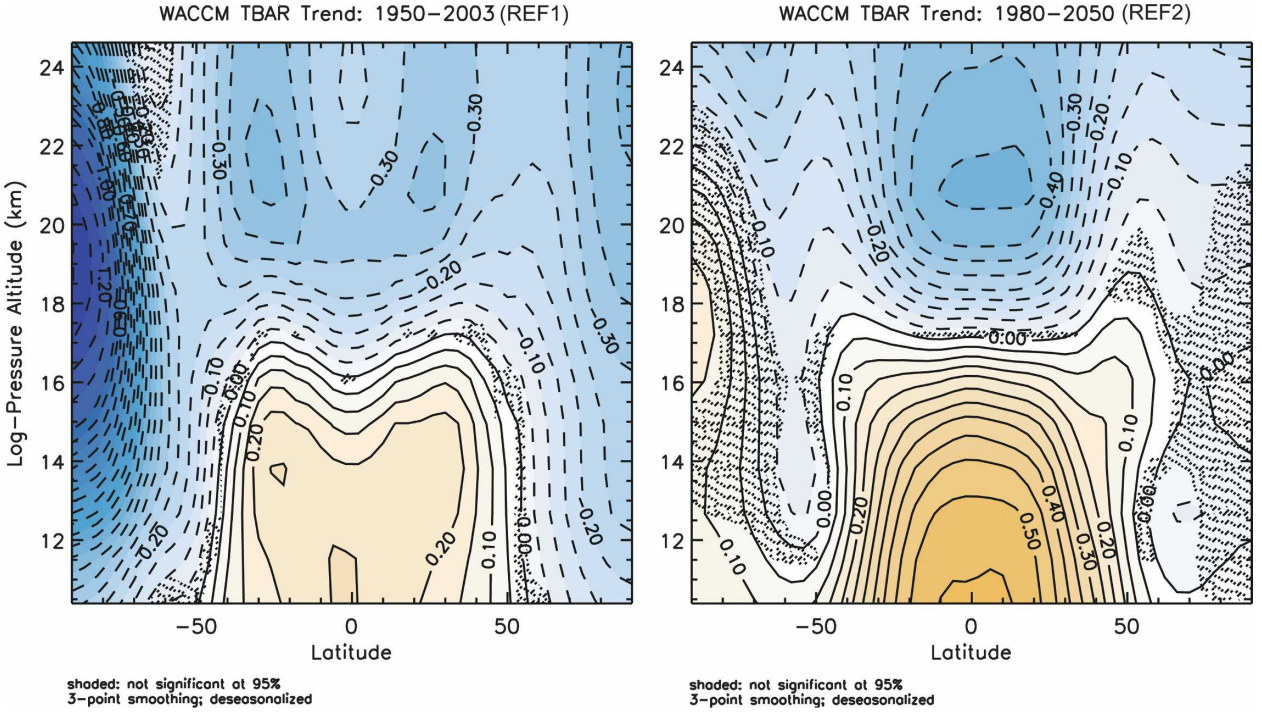

FIG. 7. As in Fig. 2, but for the ensemble-mean trends in zonal-mean temperature [contour interval is 0.05 K (10 yr)$^{-1}$] in the upper troposphere and lower stratosphere.

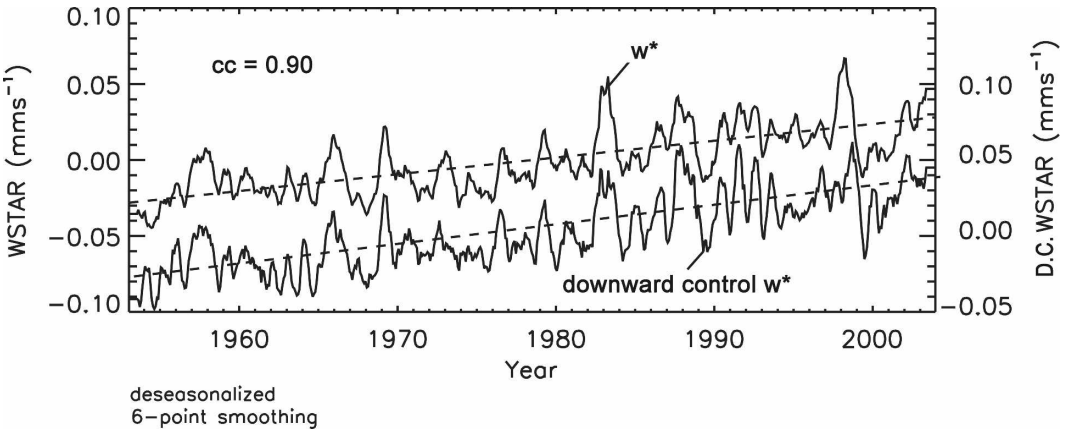

FIG. 8. Time series of ensemble-mean $\overline{w}^*$ (mm s^{-1}) in the lower stratosphere (100 hPa) averaged over the tropics (±22°) and calculated both directly (upper curve; left scale) and from the downward control principle, Eq. (1), (lower curve; right scale) for simulation REF1. The time series were deseasonalized and smoothed with a 6-point boxcar before processing. The dashed lines are the linear trend fits to the time series. The correlation coefficient between the two series is 0.90.

warming. It remains to be seen whether this leads to an increase in wave driving in the subtropical lower stratosphere in other models, as is the case in WACCM3.

In any case, in WACCM3 the mechanism outlined above is indeed robust, and it appears to operate even on much shorter time scales than those associated with the secular increase in GHG. This is illustrated in Fig. 8, which shows the tropical average of $\overline{w}^*$ in the lower stratosphere (±22°; 100 hPa) computed both directly and from the downward control principle, Eq. (1), for the REF1 simulation (which, recall, is driven by observed SST). It is evident that the major ENSO events of the twentieth century, such as those of 1957–58, 1982–83, 1997–98, and so on, are associated with positive anomalies in $\overline{w}^*$ and that the agreement between direct and downward control estimates of tropical average $\overline{w}^*$ is remarkably good. In fact, Marsh and Garcia (2007) have shown that the acceleration of the TEM circulation following ENSO events has a significant influence on tropical ozone in the lower stratosphere and that changes in the circulation lag the Niño-3.4 index (the standardized mean SST in the region 5°S–5°N, 120°–170°W) by a few months, consistent with the fact that zonal-mean warming of the troposphere during ENSO events develops after the peak in the SST anomaly. García-Herrera et al. (2006) have documented similar behavior in the BD circulation in an earlier version of WACCM, and in the "ECHAM5" model from the Max Planck Institute for Meteorology.

We note in closing that an analysis of the waves that accelerate the BD circulation in WACCM3 would shed light on the details of the mechanism described here. For example, are the waves involved synoptic-scale waves whose structure changes in response to the stronger westerlies in the lower stratosphere? Or are they planetary waves that respond to changes in the refractive properties of the background winds? To what extent do tropical waves play a role? These questions could not be addressed with the present simulations because EP fluxes were output without first performing a harmonic decomposition of the wave field. Calculations able to address these issues will be presented in a future study.

Acknowledgments. This work was supported in part by the National Aeronautics and Space Administration under Grant LWS04-0009-0122. The calculations described were performed at NCAR and on the Columbia computing system at NASA/Ames Research Center. We thank Drs. Daniel Marsh and Anne Smith and two anonymous reviewers for helpful comments and suggestions.

REFERENCES

Andrews, D. G., J. R. Holton, and C. B. Leovy, 1987: *Middle Atmosphere Dynamics.* Academic Press, 489 pp.

Austin, J., and F. Li, 2006: On the relationship between the strength of the Brewer–Dobson circulation and the age of stratospheric air. *Geophys. Res. Lett.,* **33,** L17807, doi:10.1029/2006GL026867.

Butchart, N., and A. A. Scaife, 2001: Removal of chlorofluorocarbons by increased mass exchange between the stratosphere and troposphere in a changing climate. *Nature,* **410,** 799–802.

——, and Coauthors, 2006: Simulations of anthropogenic change in the strength of the Brewer–Dobson circulation. *Climate Dyn.,* **27,** 727–741, doi:10.1007/s00382-006-0162-4.

Edmon, H. J., B. J. Hoskins, and M. E. McIntyre, 1980: Eliassen–

Palm cross sections for the troposphere. *J. Atmos. Sci.,* **37,** 2600–2616.

Eichelberger, S. J., and D. L. Hartmann, 2005: Changes in the strength of the Brewer–Dobson circulation in a simple AGCM. *Geophys. Res. Lett.,* **32,** L15807, doi:10.1029/2005GL022924.

Eyring, V., and Coauthors, 2006: Assessment of temperature, trace species, and ozone in chemistry–climate model simulations of the recent past. *J. Geophys. Res.,* **111,** D22308, doi:10.1029/2006JD007327.

——, and Coauthors, 2007: Multimodel projections of stratospheric ozone in the 21st century. *J. Geophys. Res.,* **112,** D16303, doi:10.1029/2006JD008332.

Fomichev, V. I., A. I. Jonsson, J. de Grandpré, S. R. Beagley, C. McLandress, K. Semeniuk, and T. G. Shepherd, 2007: Response of the middle atmosphere to CO_2 doubling: Results from the Canadian Middle Atmosphere Model. *J. Climate,* **20,** 1121–1144.

Garcia, R. R., D. R. Marsh, D. E. Kinnison, B. A. Boville, and F. Sassi, 2007: Simulation of secular trends in the middle atmosphere, 1950–2003. *J. Geophys. Res.,* **112,** D09301, doi:10.1029/2006JD007485.

García-Herrera, R., N. Calvo, R. R. Garcia, and M. A. Giorgetta, 2006: Propagation of ENSO temperature signals into the middle atmosphere: A comparison of two general circulation models and ERA-40 reanalysis data. *J. Geophys. Res.,* **111,** D06101, doi:10.1029/2005JD006061.

Hall, T. M., and R. A. Plumb, 1994: Age as a diagnostic of stratospheric transport. *J. Geophys. Res.,* **99,** 1059–1070.

Haynes, P. H., C. J. Marks, M. E. McIntyre, T. G. Shepherd, and K. P. Shine, 1991: On the "downward control" of extratropical diabatic circulations by eddy-induced mean zonal forces. *J. Atmos. Sci.,* **48,** 651–678.

Houghton, J. T., Y. Ding, D. J. Griggs, M. Noguer, P. J. van der Linden, X. Dai, K. Maskell, and C. A. Johnson, Eds., 2001: *Climate Change 2001: The Scientific Basis.* Cambridge University Press, 881 pp.

Marsh, D. R., and R. R. Garcia, 2007: Attribution of decadal variability in lower-stratospheric tropical ozone. *Geophys. Res. Lett.,* **34,** L21807, doi:10.1029/2007GL030935.

Olsen, M. A., M. R. Schoeberl, and J. E. Nielsen, 2007: Response of stratospheric circulation and stratosphere–troposphere exchange to changing sea surface temperatures. *J. Geophys. Res.,* **112,** D16104, doi:10.1029/2006JD008012.

Randel, W. J., R. R. Garcia, and F. Wu, 2002: Time-dependent upwelling in the tropical lower stratosphere estimated from the zonal-mean momentum budget. *J. Atmos. Sci.,* **59,** 2141–2152.

Rind, D., J. Lerner, and C. McLinden, 2001: Changes of tracer distributions in the doubled CO_2 climate. *J. Geophys. Res.,* **106,** 28 061–28 080.

Sigmond, M., P. C. Siegmund, E. Manzini, and H. Kelder, 2004: A simulation of the separate climate effects of middle-atmospheric and tropospheric CO_2 doubling. *J. Climate,* **17,** 2352–2367.

World Meteorological Organization, 2003: Scientific assessment of ozone depletion: 2002. Global Ozone Research and Monitoring Project Rep. 47, 498 pp.